On Occurrence of Mixed-torus Bursting Oscillations Induced by Non-Smoothness

Qinsheng Bi (qbi@ujs.edu.cn)
Jiangsu University https://orcid.org/0000-0002-1058-7154
Shaomin Chen
Jiangsu University

Research Article

Keywords: Non-smoothness, Coupling of different scales, Bursting oscillations, Bifurcation mechanism

Posted Date: February 28th, 2022

DOI: https://doi.org/10.21203/rs.3.rs-1360605/v1

Noname manuscript No.
(will be inserted by the editor)

On occurrence of mixed-torus bursting oscillations induced by non-smoothness

Qinsheng Bi · Shaomin Chen

Received: date / Accepted: date

Abstract The paper devotes to the slow-fast behaviors of a higher dimensional non-smooth system with the coupling of two scales. Some novel bursting attractors and interesting phenomena are presented, especially the so-called mixed-torus bursting oscillations, in which the trajectory moves along different tori in turn, though the bursting attractor still behaves in quasi-periodic form. Based on a 4-D hyper-chaotic model with two scrolls, a modified non-smooth slow-fast version is established by introducing a non-smooth boundary as well as a periodic external excitation, which can also be easily implemented by circuit. When the exciting frequency is far less than the natural frequency, implying the coupling of two scales in frequency domain exists, the whole exciting term can be regarded as a slow-varying parameter. Upon the bifurcations analysis of the subsystems in the two regions divided by the boundary, together with the non-smooth bifurcations on the boundary, the coexisted attractors with the variation of the slow-varying parameter are derived. From the dynamical evolution of the full system with the increase of the exciting amplitude, bursting oscillations may change from periodic to quasi-periodic attractor, the mechanism of which is obtained by employing the overlap of the transformed phase portrait and coexisted attractors as well as the bifurcations. Sliding along the boundary on the trajectory can be observed on the bursting attractor, the mechanism of which can be accounted for by employing the non-smooth theory or by the in-turn influence of two pseudo attractors in different regions. Supercone defined by a unstable focus may leading to the period-adding or period-decreasing phenomena in the spiking oscillations, while fold limit cycle bifurcation may result in the dramatically change of the spiking amplitude. The trajectory may pass across or graze at the boundary, while grazing bifurcation may cause the period-doubling bifurcation of the stable non-smooth limit cycle. Numerical simulation reveals that the grazing point on the trajectory can be removed by increasing the exciting amplitude, which can be used for controlling purpose. Furthermore, it is found that when the amplitude increases to an extent, both the non-smooth limit cycle as well as the cycle bifurcated from it via period-doubling bifurcation may involve the full vector field, resulting in the so-called mixed-torus bursting oscillations, in which the quiescent states seems to be pivots of the oscillations.

Keywords Non-smoothness · Coupling of different scales · Bursting oscillations · Bifurcation mechanism

Qinsheng Bi, Shaomin Chen
Faculty of Civil Engineering and Mechanics, Jiangsu University, Zhenjiang 212013, China
Qinsheng Bi, Corresponding author, E-mail: qbi@ujs.edu.cn
Shaomin Chen, E-mail: 857176591@qq.com

1 Introduction

Bursting oscillations,characterized by the combination of large-amplitude oscillations (spiking state,**SP**) and small-amplitude oscillations (quiescent state, **QS**), can often be observed in the slow-fast non-linear vector fields [1]. Generally, the bursting attractors can be classified by movement, such as periodic, quasi-periodic and chaotic bursting oscillations, or by the properties of the **QS**s and the **SP**s, such as point-cycle, cycle-cycle bursting oscillations. More commonly, they can be classified by the bifurcations at the alternations between **QS**s and **SP**s, such as fold/fold, fold/Hopf bursting oscillations [2].

The investigation of the dynamics of bursting oscillations may date back to the early 20th century for the relaxation oscillations found in singular van der Pol equation [3]. However, it was until the Nobel Prize winners, Hodgkin and Huxley, presented a slow-fast system, called Hodgkin-Huxley model, which can exhibit the activities of neuronal bursting phenomenon [4], researchers realized that the coupling of different scales is the reason for the special oscillations, which caused the behaviors of the slow-fast vector field to become one of the hot topics in nonlinear dynamics [5].

At the first stage, because of no valid theoretical method, most of the results focused on the phenomenon report of the bursting oscillations in different areas [6], or the numerical simulations for different patterns of the oscillations [7]. To reveal the mechanism of the bursting oscillations, upon the invariant manifolds [8], geometric singular perturbation theory has been developed to cope with the interaction mechanism between different scales with geometric view point [9]. For a typical autonomous slow-fast system, expressed as

$$\begin{aligned} \dot{x} &= f(x, y, \mu), \qquad \text{(Fast subsystem)} \\ \dot{y} &= \varepsilon g(x, y, \mu), \qquad \text{(Slow subsystem)} \end{aligned} \tag{1}$$

where $x \in R^M$, $y \in R^N$, $\mu \in R^K$, while $0 < \varepsilon << 1$ describes the ratio between the fast and slow scales, when $\varepsilon \to 0$, the trajectories of (1) converge during the fast epochs to the solution of the fast subsystem [10]

$$\dot{x} = f(x, y, \mu), \qquad \dot{y} = 0. \tag{2}$$

During slow epochs, on the other hand, the trajectories of (1) converge to the solution of

$$0 = f(x, y, \mu), \qquad \dot{y} = \varepsilon g(x, y, \mu), \tag{3}$$

which is differential-algebraic equation called the slow flow or the reduced system [11]. Upon the analysis of the behaviors of the fast and slow subsystems, geometric singular perturbation theory can qualitatively describe the mechanism of the dynamics of the full system [12].

Based on the theory, a slow-fast analysis method was proposed by Rinzel [13], in which the slow state variables are regarded as slow-varying parameters on the fact that the fast subsystem determines the quiescence and spiking oscillations, while the slow subsystem contributes to the modulation [14]. The attractors as well as the bifurcations of the fast subsystem with the variation of the slow-varying parameters can be derived, which can be used to account for the forms of quiescent states (QSs) and spiking states (SPs) as well as the transition mechanism between the two states [15]. By employing the method, a lot of bursting attractors have been reported [16], which can be further classified by the geometrical structures or the bifurcations [17].

The slow-fast analysis method can only be valid for the autonomous system with the coupling of two scales in time domain, in which obvious slow and fast subsystems can be obtained [18], while it cannot be used for the mechanism of the bursting oscillations in the non-autonomous system, for example, the periodically excited oscillators [19]. When there exists an order gap between the exciting frequency and the natural frequency, implying the coupling of two scales in frequency domain exists, slow-fast behaviors may also appear [20].

To investigate the mechanism of the phenomena, we proposed a modified slow-fast method [21]. For a typical vector field with excitation, written as

$$\dot{x} = f[(x, \mu, A\sin(\varepsilon\Omega t)], \tag{4}$$

where $x \in R^M$, $\mu \in R^K$, while $0 < \varepsilon << 1$, we refer to the geometric singular perturbation theory and rewrite (4) in the generalized phase space as

$$\begin{aligned} \dot{x} &= f(x, \mu, w), \qquad \text{(Fast subsystem)} \\ \ddot{w} &= -A(\varepsilon\Omega)^2 \sin(\varepsilon\Omega t), \qquad \text{(Slow subsystem)} \end{aligned} \tag{5}$$

in which w is regarded as a generalized state variable, or in the form

$$\begin{aligned} \dot{x} &= f(x, \mu, w), \qquad \text{(Fast subsystem)} \\ w &= A\sin(\varepsilon\Omega t), \qquad \text{(Slow-varying parameter)} \end{aligned} \tag{6}$$

with slow-varying parameter w. The slow-varying parameter in the modified method is expressed in the form of an algebraic equation instead of a differential equation in the traditional method, while the fast subsystem is in generalized autonomous form [22]. By regarding the slow-varying parameter as a generalized state variable, the conception of transformed phase portrait, defined by $\Gamma_G \equiv \{[x(t), w(t)] \mid t \in R\} \equiv \{[x(t), A\sin(\varepsilon\Omega t)] \mid t \in R\}$, is introduced, which can be used to describe the relationship between the state variables of the fast subsystem and the slow-varying w [23]. Combining the bifurcations of the attractors of the fast generalized autonomous subsystem with the variation of the slow-varying parameter w, one may obtain the mechanism of the bursting oscillations [24]. Based on the modified approach, several new types of bursting oscillations in periodically excited vector fields were reported, such as fold/Hopf bursting [25]. Table 1 presents the difference between the traditional slow-fast method and the modified approach.

Up to now, most of the bursting oscillations are obtained in the low dimensional smooth systems [26], in which only codimension-1 bifurcations, such as fold and Hopf bifurcations, occur at the alternations between QSs and SPs [27]. We wonder what kinds of bursting oscillations may appear in non-smooth vector field, since not only the conventional bifurcations, but also

Table. 1. The difference between the traditional slow-fast method and our modified approach

Traditional method	Modified approach
$\dot{x} = f(x, y, \mu)$	$\dot{x} = f(x, w, \mu)$
$\dot{y} = \varepsilon g(x, y, \mu)$	$w = A\sin(\varepsilon\Omega t)$
$f(x, y, \mu) = 0$	$f(x, w, \mu) = 0$
slow-varying y	slow-varying w
$\Gamma \equiv \{[x(t), y(t)] \mid t \in R\}$	$\Gamma_G \equiv \{[x(t), w(t)] \mid t \in R\}$
	$\equiv \{[x(t), A\sin(\varepsilon\Omega t)] \mid t \in R\}$

the non-conventional bifurcations, such as the multiple-crossing bifurcations, the sliding and glazing bifurcations, may take place [28].

For a non-smooth dynamical system, the non-smooth boundary divides the whole phase space into a set of regions, in which the trajectory is governed by different subsystems. According to the behaviors of the trajectory on the boundary, the switching boundary is partitioned into three different regions, i.e., the crossing region, the sliding region and the escaping region [29]. Non-conventional bifurcations at the boundary may result in special phenomena, most of which can not be observed in smooth vector fields [30]. To reveal the characteristics of these non-conventional bifurcations, a few approaches have been proposed, including the differential inclusion theory [31] and the Filippov theory [32]. These theories can be employed to investigate the behaviors of the bifurcations on the boundary, such as the bifurcations related to boundary equilibrium point and the limit cycle passing across the boundary [33], which have been widely used in many low dimensional non-smooth oscillators, especially in the planar vector fields because of the relatively simple structures of the trajectory [34]. However, it still remains a challenge how to explore the non-smooth dynamics in higher, even four, dimensional system, since there may coexist several stable attractors which may undergo different conventional and non-conventional bifurcations. Furthermore, in most published results, to simplify the analysis of the behaviors, symmetric non-smooth boundary introduced in the related papers does not violate the symmetric structures of the full vector field. For example, the symmetric two-scroll chaos remains when a symmetric super-plane boundary at $\mathbf{X} = 0$ is introduced [35].

The main purpose of the paper aims at the characteristics of bursting oscillations in a higher dimensional non-smooth oscillator with the coupling of two scales. We focus on the influence of the coexisted attractors and their related conventional and non-conventional bifurcations on the dynamical evolution when a asymmetric boundary introduced, which destroys the symmetry of the whole vector field.

In the following, based on a super-chaotic system, we establish a slow-fast non-smooth oscillator by introducing a slow-varying periodic excitation as well as a non-smooth boundary. Upon the analysis of the dynamical evolution with different distributions of the coexisted attractors and the bifurcations, some novel bursting attractors as well as the mechanism are presented, in which a few interesting phenomena such as the period-increasing (decreasing) and mixed-torus structures can be found.

2 Mathematical model

Since the hyper-chaotic system with more than one positive Lyapunov exponent may exhibit complicated behaviors, a lot of such oscillators have been established, among which a new 4-D vector field with two scrolls was proposed in the form [35]

$$\begin{aligned} \dot{x_1} &= a(x_2 - x_1) + bx_2x_3 + x_4, \\ \dot{x_2} &= cx_2 - x_1x_3^2 - x_4 + w, \\ \dot{x_3} &= \alpha x_3 + \beta x_1^2 + x_1x_2 + g(x), \\ \dot{x_4} &= x_1 + \gamma x_4, \end{aligned} \tag{7}$$

with $w = 0$ and $g(x) = 0$. Numerical simulations as well as electronic circuit experiment show that the multi-stability leads to the two-scroll hyper-chaotic attractor with the variation of the parameters. We refer to the system for the reasons as

- It may display two-scroll hyper-chaotic attractor with two positive Lyapunov exponent for certain parameter values.
- It can be easily implemented by electronic circuit.
- The dimension of the vector field is relatively high.
- The vector field is symmetric under the transformation $(x_1, x_2, x_3, x_4) \to (-x_1, -x_2, x_3, -x_4)$.
- Coexisted stable attractors can be observed with the variation of parameters.

In order to investigate the influence of the multi-stability and possible regular and non-regular bifurcations the dynamics when the coupling of two scales and non-smoothness exist simultaneously, here we introduce a slow-varying external excitation and a non-smooth term, expressed in the forms $w = A\sin(\varepsilon\Omega t)$ and $g(x) = -3\mathrm{sgn}(\mathrm{x} - 1)$, respectively. When the exciting frequency $\varepsilon\Omega$ is far less than the natural frequency of the system, denoted by ω_N, the coupling of two scales in frequency domain exists. Furthermore, the asymmetric non-smooth boundary, defined as $\Sigma \equiv \{(x_1, x_2, x_3, x_4) \mid x_1 = 1\}$, divides the phase space into two regions, described by $D_+ \equiv \{(x_1, x_2, x_3, x_4) \mid$

$x_1 > 1\}$ and $D_- \equiv \{(x_1, x_2, x_3, x_4) \mid x_1 < 1\}$, in which the trajectory is governed by two different subsystems, respectively.

Remark: The natural frequency of a nonlinear system may vary with its behaviors. For example, when the trajectory tends to a stable focus, it can be approximated by the imaginary part of the pair of conjugate eigenvalues, while when the trajectory oscillates around a limit cycle, it can be computed at the frequency of the cycle.

As we have mentioned in above section and our other papers, for $0 < \varepsilon\Omega \ll 1$, the whole exciting term $w = A\sin(\varepsilon\Omega t)$ can be regarded as a generalized state variable, which forms the slow subsystem, leading to the so-called fast subsystem in generalized autonomous form. In order to reveal the mechanism of the dynamics of full system, now we turn to the attractors and their bifurcations of the fast subsystem with the variation of the slow-varying parameter w.

3 Bifurcation of the generalized autonomous fast subsystem

The generalized autonomous fast subsystem can be further expressed in the form

$$\dot{\mathbf{X}} = \begin{cases} F_+(\mathbf{X}, w) = (f_1^+, f_2^+, f_3^+, f_4^+)^T, \ \mathbf{X} \in D_+, \\ F_-(\mathbf{X}, w) = (f_1^-, f_2^-, f_3^-, f_4^-)^T, \ \mathbf{X} \in D_-, \end{cases} \tag{8}$$

which implies the trajectory of the fast subsystem is governed by different subsystems when it is located in different regions $D_\pm$. Therefore, we need to investigate the bifurcations of the two subsystems defined in the two regions $D_\pm$ as well as the whole fast subsystem, respectively. Here for simplicity we denote the full nonsmooth generalized autonomous fast subsystem in (7) by FS_0 and its two subsystems by $FS_\pm$, located in $D_\pm$, respectively.

Symmetric structures can be found in both the two subsystems $FS_\pm$ since they keep unchanged under the transformation

$$(x_1, x_2, x_3, x_4, t) \to (-x_1, -x_2, x_3, -x_4, \pi/(\varepsilon\Omega)+t). \tag{9}$$

To simplify the analysis, here we fix the parameters at

$$a{=}1.0, b{=}3.0, c{=}{-}1.0, \alpha{=}{-}4.0, \beta_1{=}1.0, \gamma_1{=}{-}3.0, \tag{10}$$

to derive the equilibrium branches and their bifurcations of the three subsystems FS_0 and $FS_\pm$ with the variation of the slow-varying parameter w.

3.1 Equilibrium state and the bifurcations of the subsystems $FS_\pm$ in $D_\pm$

For the subsystem in D_+ with $g(x) = -3$, the equilibrium point can be written as $E_+(X_{1+}, X_{2+}, X_{3+}, X_{4+})$, where X_{1+} satisfies

$$\begin{aligned} &243X_{1+}^9 - 648wX_{1+}^6 + 1847X_{1+}^7 - 8928wX_{1+}^4 \\ &\quad +4137X_{1+}^5 + 6165X_{1+}^3 + 10368w^2X_{1+} \\ &\quad -10008wX_{1+}^2 - 1728w + 6264X_{1+} = 0, \end{aligned} \tag{11}$$

while

$$\begin{aligned} X_{2+} &= \triangle_+, \\ X_{3+} &= X_{1+}(X_{1+} + \triangle_+)/4 - 3/4, \\ X_{4+} &= X_{1+}/3, \end{aligned} \tag{12}$$

with

$$\triangle_+ = \frac{-9X_{1+}^5 + 46X_{1+}^3 + 144w - 129X_{1+}}{3(3X_{1+}^4 - 13X_{1+}^2 + 48)}. \tag{13}$$

Similarly, the equilibrium point in D_- can be expressed as $E_-(X_{1-}, X_{2-}, X_{3-}, X_{4-})$, where X_{1-} satisfies

$$\begin{aligned} &-81wX_{1-}^6 - 29X_{1-}^7 - 630wX_{1-}^4 - 753X_{1-}^5 \\ &\quad +1296w^2X_{1-} - 441wX_{1-}^2 - 3303X_{1-}^3 \\ &\quad +5616w - 6183X_{1-} = 0, \end{aligned} \tag{14}$$

while

$$\begin{aligned} X_{2-} &= \triangle_-, \\ X_{3-} &= X_{1-}(X_{1-} + \triangle_-)/4 + 3/4, \\ X_{4-} &= X_{1-}/3. \end{aligned} \tag{15}$$

with

$$\triangle_- = \frac{-9X_{1-}^5 - 62X_{1-}^3 + 144w - 129X_{1-}}{3(3X_{1-}^4 + 5X_{1-}^2 + 48)}. \tag{16}$$

The stability of the equilibrium points can be uniformly determined by the associated characteristic equation, written in the form

$$\lambda^4 + 9\lambda^3 + q_2\lambda^2 + q_1\lambda + q_0, \tag{17}$$

where

$$\begin{aligned} q_2 &= 2X_{1\pm}^2X_{3\pm} + 3X_{3\pm}^3 - 6X_{1\pm}X_{2\pm} - 3X_{2\pm}^2 \\ &\quad +X_{3\pm}^2 + 26, \\ q_1 &= 12X_{1\pm}^2X_{3\pm}^2 + 9X_{1\pm}X_{2\pm}X_{3\pm}^2 + 12X_{1\pm}^2X_{3\pm} \\ &\quad +2X_{1\pm}X_{2\pm}X_{3\pm} + 21X_{3\pm}^3 - 24X_{1\pm}X_{2\pm} \\ &\quad -12X_{2\pm}^2 + 7X_{3\pm}^2 + 3X_{3\pm} + 27 \\ q_0 &= 36X_{1\pm}^2X_{3\pm}^2 + 27X_{1\pm}X_{2\pm}X_{3\pm}^2 + 16X_{1\pm}^2X_{3\pm} \\ &\quad +6X_{1\pm}X_{2\pm}X_{3\pm} + 36X_{3\pm}^3 - 15X_{1\pm}X_{2\pm} \\ &\quad -9X_{2\pm}^2 + 12X_{3\pm}^2 + 12X_{3\pm} + 12. \end{aligned} \tag{18}$$

The equilibrium point is stable if $\mathrm{Re}(\lambda_\mathrm{i}) < 0, \mathrm{i} = 1, 2, 3, 4$, which may lose its stability via two types of codimension-1 bifurcations. Fold bifurcation may occur when one

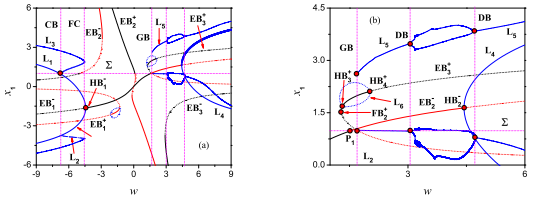

Fig. 1. Equilibrium branches and their bifurcations of the generalized autonomous fast subsystem FS_0 and the related two subsystems $FS_\pm$ located in $D_\pm$ respectively in (a) with locally enlarged part in (b). All the equilibrium branches in red are pseudo equilibrium branches on the fact that the locations of these equilibrium branches and the corresponding governing subsystems are defined in different regions. The attractors in solid line and dotted line represent stable and unstable ones, respectively

zero eigenvalues appears, resulting in the jumping phenomenon between different equilibrium points, while Hopf bifurcation may take place when a pair of pure imaginary eigenvalues can occur, leading to the periodic oscillations.

Because of the complicated expressions of the equilibrium points as well as the characteristic equation, we now turn to the numerical simulations.

Fig.1 gives the steady states of the generalized autonomous fast subsystem FS_0 and the two subsystems $FS_\pm$ in $D_\pm$ with the variation of the slow-varying parameter w.

We first focus on the subsystem FS_+ in D_+. With the variation of w, the equilibrium points form three equilibrium branches, denoted by $EB_i^+, i = 1, 2, 3$, seeing Fig.1. Because of the symmetry of FS_+, Table 2 only presents the dynamical behaviors for $w \leq 0$, while the details for $w > 0$ is omitted here for simplicity.

Note: All the equilibrium points on EB_1^+ are pseudo equilibrium points, while the number of equilibrium point on E_3^+ varies from one to three, which may appear as admissible or pseudo equilibrium points, depending on the relationship between the their locations and the non-smooth boundary.

For the subsystem FS_+ in D_+, a stable node, a unstable focus and a unstable saddle can be observed when $w \in (-\infty, -2.1218)$, shown in Fig.2 for $w = -6.82$. Two hetero-clinic orbits, denoted by $S_{1,2}$, can be observed. S_1 connects the unstable focus E_1^+ and the stable node E_3^+, while S_2 connects the saddle point E_2^+ and the stable node E_3^+.

Computation reveals that at $w = -2.1218$ and $w = -1.2394$, subcritical Hopf bifurcations occur, causing

Table. 2. Table Dynamical behaviors of FS_+ with the variation of s

Slow-varying parameter	Dynamical behavior
$w \in (-\infty, -2.1218)$	an unstable focus and a saddle on EB_1+, together with a stable node on EB_2^+
$w = -2.1218$	subcritical Hopf bifurcation at the focus on EB_1+
$w \in (-2.1218, -1.2394)$	a stable focus and a saddle on EB_1+, together with a stable node on EB_2^+
$w = -1.2394$	subcritical Hopf bifurcation at the focus on EB_1+
$w \in (-1.2394, -1.2386)$	an unstable focus and a saddle on EB_1+, together with a stable node on EB_2^+
$w = -1.2386$	saddle-focus bifurcation
$w \in (-1.2386, -0.1560)$	a stable node on EB_2^+
$w = -0.1560$	saddle-node bifurcation
$w \in (-0.1560, 0]$	two stable node and a saddle EB_2^+

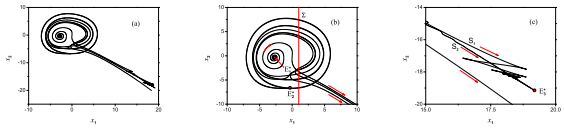

Fig. 2. Project of the phase portrait on the (x_1, x_2) plane without the non-smooth boundary Σ for $w = -6.82$ in (a) with locally enlarged parts in (b) and (c).

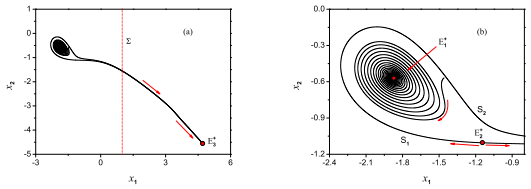

Fig. 3. Project of the phase portrait on the (x_1, x_2) plane without the non-smooth boundary Σ for $w = -1.50$ in (a) with locally enlarged part in (b).

the qualitative changes of the phase portrait on the phase space. When $w \in (-2.1218, -1.2394)$, a stable focus E_1^+, an unstable saddle E_2^+ and a stable node E_3^+ can be observed, where two hetero-clinic orbits $S_{1,2}$ connect E_2^+ and E_3^+, shown in Fig.3 for $w = -1.50$.

When $w \in (-1.2394, -1.2386)$, the stable focus E_1^+ changes to a unstable one via subcritical Hopf bifurcation, which meets the saddle point E_2^+ at $w = -1.2386$ to form a saddle-focus bifurcation, leading to the disappearance of the two equilibrium points.

When $w \in (-1.2386, -0.1560)$, only one stable node E_3^+ exists. Fold bifurcation in type of saddle-node at $w = -0.1560$ results in the occurrence of a saddle E_1^+

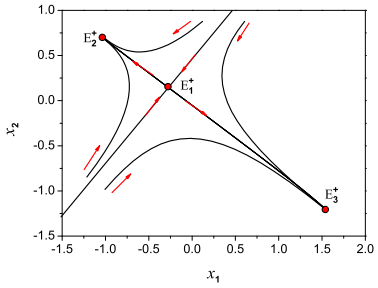

Fig. 4. Project of the phase portrait on the (x_1, x_2) plane without the non-smooth boundary Σ for $w = -0.10$.

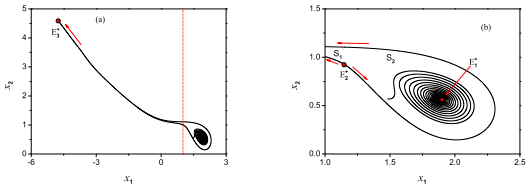

Fig. 5. Project of the phase portrait on the (x_1, x_2) plane for $w = +1.50$ without the non-smooth boundary Σ in (a) with locally enlarged part in (b).

and a stable node E_2^+, leading to two stable node and a saddle for $w \in (-0.1560, +0.1560)$, seeing Fig.4 for $w = -0.10$

Symmetrically behaviors can be observed for $w \in (0, +\infty)$. For example, subcritical Hopf bifurcations at $w = +1.2394$ and $w = +2.1218$ lead to the alternation of E_1^+ between a stable and an unstable focus, seeing Fig.5 for $w = +1.50$, with two hetero-clinic orbits $S_{1,2}$ connecting E_2^+ and node E_3^+, respectively.

Remark: Though the dynamical behaviors are symmetric about $w = 0.0$, some of the equilibrium points may change between pseudo and admissible equilibrium points because of the locations of the points may change with the variation of w.

Now we turn to the subsystem FS_- in D_-. With the variation of w, the equilibrium points form also three equilibrium branches, denoted by $EB_i^-, i = 1, 2, 3$, seeing Fig.1. Table 3 presents the equilibrium points as well as the bifurcations of FS_- with the variation of w for $w \le 0$, while the details for $w \ge 0$ are omitted because of the symmetry.

For $w \in (-\infty, -4.4363)$, a stable node and a unstable node on EB_2^- can be observed, which is coexisted with a stable limit cycle L_1 bifurcated from a unstable focus on EB_1^-, seeing Fig.6a for $w = -6.82$.

Table. 3. Dynamical behaviors of FS_- with the variation of w

Slow-varying parameter	Dynamical behaviors
$w \in (-\infty, -4.4363)$	a stable node and a unstable node on EB_2^-, a stable limit cycle L_1 oscillating around a unstable focus on EB_1^-
$w = -4.4363$	supercritical bifurcation at the focus on EB_1^-
$w \in (-4.4363, -2.9179)$	a stable node and a unstable node on EB_2^-, a stable focus on EB_1^-
$w = -2.9179$	node-node bifurcation on EB_2^-
$w \in (-2.9179, 0.0]$	a stable focus on EB_1^-

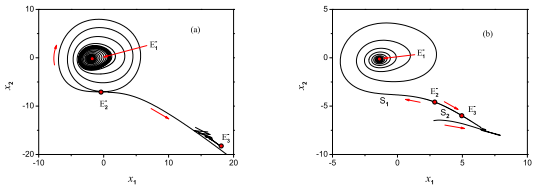

Fig. 6. Projects of the phase portrait on the (x_1, x_2) plane without the non-smooth boundary Σ. (a)$w = -6.82$; (b) $w = -3.0$.

The limit cycle may disappear via supercritical Hopf bifurcation at $w = -4.4363$, at which the unstable focus changes to be a stable one, seeing Fig.6b for $w = -3.0$. It can be observed that there exist two hetero-clinic orbits, denoted by $S_{1,2}$, where S_1 connects the stable focus E_1^+ and the unstable node E_2^+, while S_2 connects the point E_2^+ and the stable node E_3^+.

With the increase of w, E_2^+ moves towards E_3^+, and finally meet E_3^+ at $w = -2.9179$ to form a node-node bifurcation, resulting in the disappearance of the two nodes, which leads to only a stable focus for $w \in (-2.9179, 0.0)$.

Remark: Some of the equilibrium points may change between pseudo and admissible equilibrium points because of the locations of the points may change between $D_\pm$ with the variation of w. Furthermore, because of the high dimension of the system, it is very difficult to obtain exactly the attracting basins of the stable attractors.

3.2 Bifurcation of the full non-smooth generalized autonomous fast subsystem FS_0

Now we turn to the full non-smooth generalized autonomous fast subsystem FS_0. From the non-smooth

Table. 4. Dynamical behaviors of FS_0 with the variation of w

Slow-varying parameter	Dynamical behaviors
$w \in (-\infty, -6.8203)$	a stable limit cycle L_3 and a stable node on EB_2^+
$w = -6.8203$	C-Bifurcation
$w \in (-6.8203, -4.5433)$	two stable limit cycles L_1 an L_3, together with a stable node on EB_2^+ and a unstable limit cycle L_2
$w = -4.5433$	fold limit cycle bifurcation of L_2 and L_3
$w \in (-4.5433, -4.4363)$	a stable limit cycle L_2 and a stable node on EB_2^+
$w = -4.4363$	Hopf bifurcation on EB_1^-
$w \in (-4.4363, +1.6990)$	a stable focus on EB_1^- and a stable node on EB_2^+
$w = +1.6990$	grazing bifurcation
$w \in (+1.6990, +3.0656)$	a stable grazing limit cycle L_5
$w = +3.0656$	period-doubling bifurcation
$w \in (+3.0656, +4.7195)$	period-doubling oscillations
$w = +4.7195$	period-doubling bifurcation
$w \in (+4.7195, +\infty)$	a stable crossing limit cycle L_5

boundary $h(x) = x = 1$, we can compute the directional Lie derivative as $L_{F_\pm} =< \nabla h, F_\pm >= f_1^\pm$. Setting $L_{F_\pm} = 0$ yields the set of tangent singular points, represented by $\Gamma \equiv \{(x_1, x_2, x_3, x_4) \mid \mathbf{X} \in \Sigma, f_1^\pm = 0\}$. Since $f_1^+ = f_1^-$, Therefore, for a given value of w, when the trajectory reaches the non-smooth boundary at the point $\mathbf{X}_0 \in \Sigma$, if $f_1^\pm = 0$, sliding or grazing phenomenon can be observed. Otherwise, the trajectory may pass across the boundary. Furthermore, with a small perturbation of the parameters, if the value of $f_1^\pm = 0$ keeps at zero, the trajectory may sliding along the boundary; otherwise, a grazing point on the trajectory can be observed.

Now we turn to the numerical simulations for non-smooth bifurcations. Table 4 shows the attractors in the FS_0 with the variation of w.

Fig.7 gives the solutions of FS_0 and $FS_\pm$ for $w = -7.0$. For the subsystem FS_+ in D_+, there exists a hetero-clinic orbit S connecting the unstable focus E_1^+ and the stable node E_3^+. While for the subsystem FS_- in D_2, the trajectory may approach a stable limit cycle L_1, which have two interaction points M_2 and M_3 with the non-smooth boundary Σ. When the trajectory of FS_0 is located in D_-, it is governed by FS_- and tends to the stable limit cycle L_1. When it arrives at the point M_2 in Fig.7a, since dx_1/dt keeps positive, seeing Fig.7b, it passes across the boundary to enter D_+. Then the trajectory turns to be governed by FS_+. Affected by the hetero-clinic orbit, the trajectory moves along the orbit of the unstable focus. When it returns to boundary,

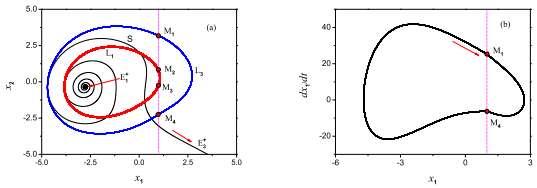

Fig. 7. Oscillations of the three subsystem FS_0 and $FS_\pm$ for w=-7.0. (a) Projects of the phase portrait on the (x_1, x_2) plane of the three subsystems;(b) The variation of x_1 on the $(x_1, dx_1/dt)$ plane.

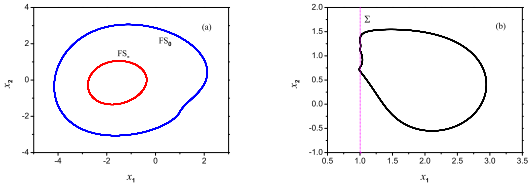

Fig. 8. Phase portrait on the (x_1, x_2) plane of the subsystem FS_0. (a) w=-5.0; (b) w=+2.0.

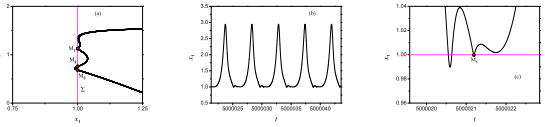

Fig. 9. Oscillations of the subsystem FS_0. (a) Locally enlarged phase portrait on the (x_1, x_2) plane; (b) Time history of x_1 with locally enlarged part in (c).

it also passes across because of the same reason. The alternated influence may finally reach a balance, leading to a non-smooth limit cycle L_3 in FS_0.

Fig.8 gives the phase portraits on the (x_1, x_2) plane of FS_0 for $w = -5.0$ and $w = +2.0$, respectively. Note that when $w = -5, 0$, the stable limit cycles L_1 and L_3 coexist, corresponding to different attracting basins. However, because of the grazing bifurcation at $w = +1.6990$, a grazing limit cycle can be observed for $w = +2.0$, seeing Fig.8b.

From the enlarged phase portrait in Fig9a, one may find that there exists two types of the behaviors when the trajectory arrives at the non-smooth boundary. It may graze the non-smooth boundary, seeing point M_1 in Fig.9a. For the case, one may find from the time history of x_1 in Fig.9b and Fig.9c that the value of x_1 at M_1 reaches its extreme value, implying $dx_1/dt = 0$, which agrees well with the theoretical result. It may also passes directly across the boundary, seeing points M_2 and M_3 in Fig.9a, at which the related values of dx_1/dt keep the sign, demonstrated by the time history of x_1 in Fig.9c.

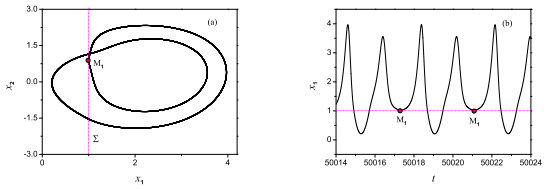

Fig. 10. Period-2 oscillations of the subsystem FS_0 for $w = +4.0$. (a) Phase portrait on the (x_1, x_2) plane; (b) Time history of x_1.

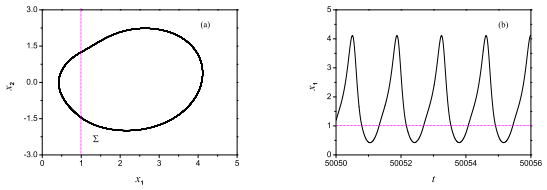

Fig. 11. Period-1 oscillations of the subsystem FS_0 for $w = +6.0$. (a) Phase portrait on the (x_1, x_2) plane; (b) Time history of x_1.

With the increase of the parameter w, period-doubling bifurcation can be observed for FS_0, seeing Fig.10 for $w = +4.0$. During each period, there exist two crossing points and a grazing point on the trajectory.

Further increase of w may cause the disappearance of the grazing point, leading to period-1 oscillations, shown in Fig.11 for $w = +6.0$.

Period-adding phenomenon Numerical simulation reveals that both the periods of the two limit cycles L_1 and L_3 change slowly with the variation of w, which is almost similar to the phenomenon observed for the limit cycle in smooth vector field. However, the period of the limit cycle L_5 changes dramatically with the variation of w. The limit cycle L_1 via Hopf bifurcation at HB_1^- in Fig.1 is governed by the subsystem FS_- in D_-, the amplitude of which increases with the decrease of w. When it reaches the boundary, C-bifurcation occurs, leading to the stable non-smooth limit cycle L_3, which causes the abrupt increase of the oscillating amplitude. However, small change of the period can be observed between the two cycles L_1 and L_3 , since most part of the non-smooth limit cycle L_3 is still governed by the subsystem FS_-, while the other part is determined by the flow around the focus E_1^+ in D_+, seeing Fig.2b and Fig.7.

Now we focus on the limit cycle L_5 via grazing bifurcation at the boundary. From the stability analysis of the equilibrium branches, one may find, when the trajectory is located in region D_-, it may passes across the boundary to enter region D_+. Once the trajectory

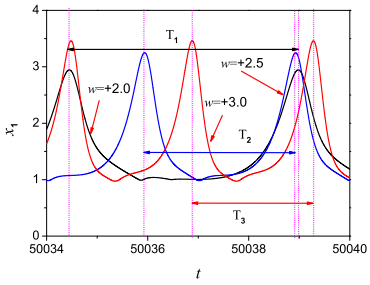

Fig. 12. Comparison between the three cases. (a) Phase portrait on the (x_1, x_2) plane; (b) Time history of x_1.

is located in D_+, it will be governed by the subsystem FS_+, the phase portrait of which is symmetric to that in Fig.2. Before the period-doubling bifurcation occurs, the trajectory is mainly governed by the subsystem FS_+ except in the small neighborhood of the grazing point. Note that the flow surrounding the unstable focus on EB_3^+ in Fig.1b forms a super-cone. With the variation of w, a set of super-cones surrounding the focus on the equilibrium branch EB_3^+ exist. Since the trajectory moves according to different super-cones for different values of w, abrupt change of period of the limit cycle can be observed, leading to the period-adding/decreasing phenomenon with the slow-varying w.

Period-doubling phenomenon For the value of w, there exist two hetero-clinic orbits connecting a stable in D_- and an unstable node in D_+, which implies there exist two possible routes for the trajectory from any initial point located in D_+ to approach the stable node in D_-, when the non-smooth boundary does not exist, shown in Fig.5. Therefore, two possible intersection points between the trajectory and Σ may be observed. When only one of the possible intersection points appear, which behave in grazing type, period-1 solution can be observed, seeing N_3 in Fig.13a for $w = +2.0$, while the other point just approaches the boundary, seeing N_1 in Fig.13a. With the increase of w, the inertia of the movement increases, causing the original N_1 to arrives at the boundary. Because of the characteristics of the vector field, no singular property of the intersection point exists, which causes the trajectory to pass directly across the boundary, yielding two more intersection points on the boundary, resulting in period-doubling bifurcation, seeing Fig.13b for $w = +4.0$.

Further increase of w may continue to increase the vibration intensity, causing the trajectory at N_3 to directly passes across the boundary, which lead to the dis-

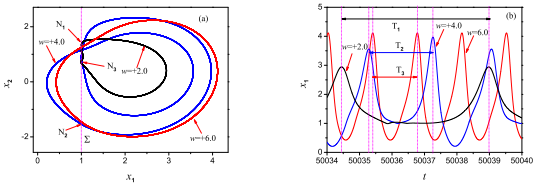

Fig. 13. Comparison between the three cases. (a) Phase portrait on the (x_1, x_2) plane; (b) Time history of x_1.

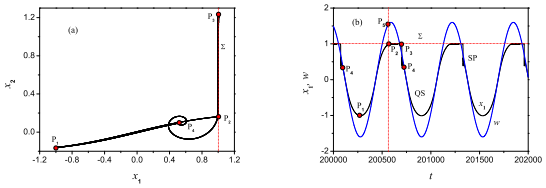

Fig. 14. Non-smooth bursting oscillations for $A = 1.60$. (a) Phase portrait on the (x, y) plane; (b) Time histories of x and w.

appearance of the grazing point on the trajectory. For the situation, period-1 solution can be observed, which implies the trajectory may pass across the boundary only via the two possible point.

Remark: Here we would like to point out that the super-cone determined by the stable or unstable focus may be one of the reasons for the period-decreasing or period-increasing phenomenon of the periodic oscillations in the non-smooth vector field. Furthermore, the grazing point may be eliminated by the increase the vibration intensity, which can be used for controlling purpose.

From above analysis, one may find that for a non-smooth vector field, there exists different attractors as well as regular and non-smooth bifurcations, which leads to different distributions of the attractors and the bifurcations with the variation of w. In the following, we will investigate the slow-fast behaviors when the coupling of two scales in frequency involves the full system.

4 Evolution of the dynamics

Note that the slow-varying parameter w may change between $-A$ and $+A$ periodically for a given exciting amplitude A. With the increase of the exciting amplitude, different types of attractors and their bifurcations may involve the full system, resulting in qualitatively different behaviors. Now we focus on the dynamical evolution with the increase of the exciting amplitude.

Since the distance between some bifurcation points is very short, to display the influence of all possible stable attractors of the generalized autonomous fast subsystem on the dynamics of the full system, we need the variable w to change slowly enough. For the purpose, here we fix the exciting frequency $\varepsilon\Omega$ at $\varepsilon\Omega = 0.001$.

Remark: Numerical simulations demonstrate that when the small parameter $\varepsilon\Omega$ is taken a bit large, some of the behaviors may disappear, since w passes across the region confined by the associated bifurcation points with short distance along w-axis before the influence of the bifurcations occurs.

It can be found that the the stable EB_1^- meet the non-smooth boundary at $w = 1.5536$, seeing Fig.1. Therefore, for $A \in (0, 1.5536)$, though there exist a few bifurcations, such as node-node bifurcation and the subcritical Hopf bifurcation, the full system appears in limit cycle with the same frequency as that of the excitation, since the trajectory of the full system does not pass across the boundary Σ, implying the full system oscillates around the equilibrium branch EB_1^- governed by the subsystem in D_-, which we omit here for simplicity, seeing Fig.1.

4.1 Periodic relaxation oscillations with sliding

For $A = 1.5536$, EB_1^- reaches the non-smooth boundary, causing the trajectory to slide along the non-smooth boundary, seeing Fig.14 for $A = 1.60$. The dynamics behaves in periodic oscillations with the same period as that of the excitation, the trajectory for each period of which can be divided into three segments, denoted by P_1P_2, P_2P_3 and P_3P_4, where the segment P_2P_3 is located on the boundary while repetitive spiking oscillations can be observed around the point P_4.

To reveal the mechanism of the non-smooth bursting oscillations, we turn to the overlap of the transformed phase portrait and equilibrium branches as well as their bifurcations on the (w, x_1) plane, shown in Fig.15a.

With the increase of the slow-varying parameter w, the trajectory, starting from the point P_1 with minimum value of w at $w = -1.60$, moves almost strictly along the stable segment of equilibrium branch EB_1^-, behaving in quiescent state, since the trajectory is governed by the subsystem in D_-. When the trajectory reaches the non-smooth boundary Σ at P_5, it slides along Σ because of the sliding bifurcation. When w increases to the maximum value with $w = +1.60$ at P_2, the trajectory turns to the left. It then moves almost strictly along Σ to the point P_3, at which non-

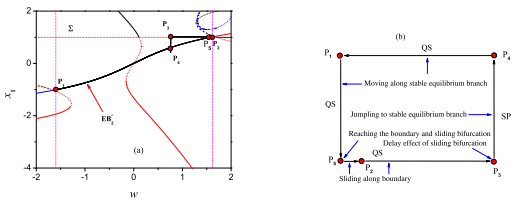

Fig. 15. (a) Overlap of the transformed phase portrait and equilibrium branches on the (w, x_1) plane; (b) Structure of the bursting attractor for $A = 1.60$.

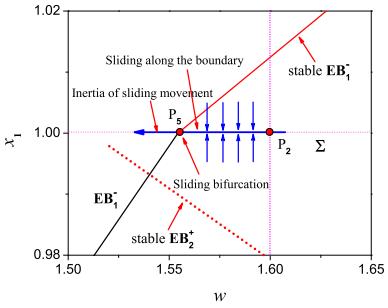

Fig. 16. Sliding mechanism.

smooth sliding bifurcation occurs. The trajectory jumps to the stable segment of equilibrium branch EB_2^-, yielding repetitive spiking oscillations. The trajectory finally settles down to the stable equilibrium branch at the point P_4, and turns to move almost strictly along the stable equilibrium branch. When the trajectory arrives at the point P_1, one period of the oscillations is finished.

The structure of the bursting oscillations is presented in Fig.15b, which can be can be called periodic non-smooth relaxation oscillations with sliding, because of the sliding bifurcation at the transitions between the boundary and the stable equilibrium branches.

Spiking oscillations When the trajectory along the boundary enters the region D_-, it may tend to the stable equilibrium branch of the subsystem in D_-, which is of focus type. Therefore, the spiking oscillations can be approximated by the transient process from the point on the boundary to the focus on the equilibrium branch EB_1^- for the corresponding value of w.

Sliding mechanism Once the trajectory moving along the stable equilibrium segment EB_1^- of the subsystem in D_- reaches the non-smooth boundary Σ at P_5, it then turns to move along the boundary, resulting in sliding phenomenon. From the time history of x_1 and w in Fig.14b, one may find when the trajectory along EB_1^- reaches the boundary at P_5 with $x_1 = 1.0$, the value of w at P_5 can be approximated at $w = 1.5818$, which implies w may still increase with the evolution of time since $A = 1.60$. Theoretically, without the boundary, the trajectory passes across the boundary and enters the region D_+. Because of the boundary, when the trajectory passes across the boundary, it turns to be governed by the subsystem FS_+ in D_+. Since the associated stable equilibrium branch EB_2^+ of the system in D_+ is located in D_-, though it is a pseudo stable equilibrium branch, it still attracts the trajectory, causing the trajectory to return to the region D_-, seeing Fig.16. When the trajectory passes across the boundary to enter the region D_-, it then is governed by the subsystem FS_- in D_-. Note that for $w \in (1.5818, 1.60]$, the stable equilibrium points EB_1^- of the subsystem FS_- is located in D_+, which causes the trajectory to return to region D_+. Skipping the transient process, the back and forth influence of the two governing subsystems $FS_\pm$ finally causes the trajectory to move along the non-smooth boundary, leading to the sliding phenomenon. When the slow-varying parameter w decreases from the maximum value $w = 1.60$, because of the inertia of the movement along the boundary, the trajectory may still move along the boundary for a segment until the effect of sliding bifurcation occurs, seeing Fig.16.

The sliding mechanism can also be demonstrated by the non-smooth theory. When $w \in (-1.5818, 1.60)$, for the trajectory in D_+, x_1 may decrease because of the stable equilibrium branches EB_2^+, while for the trajectory in D_-, x_1 may increase because of the stable EB_1^-. Assuming the trajectory from $D_\pm +$ arrives at Σ at the point $\mathbf{X}_\pm$, one may find $f_1^+(\mathbf{X}_+) < 0$ and $f_1^-(\mathbf{X}_-) > 0$, which implies the segment $w \in (-1.5818, 1.60)$ on w-axis corresponds to the sliding region, with sliding bifurcation at P_5.

Remark: Numerical simulation reveals that there still exist fluctuations during the sliding passage because of the inertia of the movement. The fluctuations may finally disappear when long enough transient process is skipped. It is noticed that there exists delay effect of the sliding bifurcation at P_5 because of the slow passage influence caused by the inertia of the movement along the boundary, which causes the jumping phenomenon to occur at P_3 instead of P_5.

4.2 Periodic point-cycle bursting oscillations

With the increase of the exciting amplitude, when $A = 1.6990$, grazing bifurcation at $w = +1.6990$ may involve the dynamics, leading to the qualitative change of the behavior, seeing Fig.17 for $A = 1.70$. From the phase portrait in Fig.17a, one may find that the topological

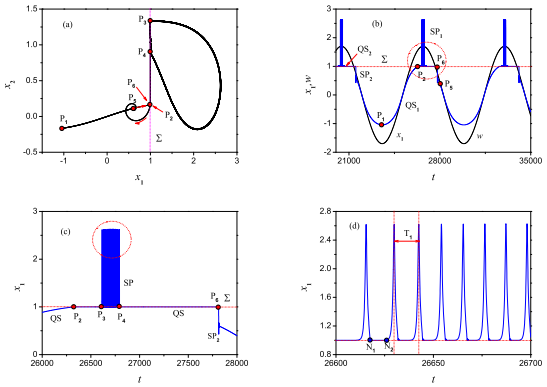

Fig. 17. Periodic non-smooth point-cycle bursting oscillations for $A = 1.70$. (a) Phase portrait on the (x_1, x_2) plane; (b) Time histories of x_1 and w, with locally enlarged parts of time history of x_1 in (c) and (d).

structure of the part of the trajectory located in the region D_- is the same as that in Fig.15a, since the trajectory is governed by the same subsystem FS_-. However, instead of sliding along the boundary, for larger exciting amplitude, the trajectory, not only slides along the boundary, but also passes across the boundary to oscillate according to a cycle, yielding repetitive spiking oscillations, seeing SP in Fig.17c, since stable non-smooth limit cycle meets the boundary at $w = +1.6916$ to yield grazing bifurcation.

From the time history in Fig.17b, one may find that, the trajectory for one period can be divided into four segments, corresponding to two quiescent state and two spiking state. The trajectory in spiking state for the part P_3P_4, denoted by SP_1, oscillates according to the non-smooth limit cycle, while the trajectory in the part P_6P_5, denoted by SP_2, corresponds to the transient process from the point on the boundary to a stable focus. The quiescent QS_1 for the trajectory from P_1 to P_3 is composed of two parts, where the trajectory in P_1P_2 moves along the stable equilibrium branches of the subsystem in D_-, while in P_2P_3, it slides along the boundary. The trajectory in quiescent state QS_2 from P_4 to P_6 just moves along the boundary, shown in Fig.17c and Fig.17d.

Furthermore, the frequency of SP_1 can be approximated by the frequency of the non-smooth limit cycle at $\Omega_1 = 0.5148$, while the frequency of SP_2 can be approached by the imaginary part of the pair of complex conjugate eigenvalues at $\Omega_2 = 2.0944$, both of which agree with the numerical results. For example, from the time history in Fig.17d, the frequency of SP_1 can be computed at $\Omega_1 = 2\pi/T_3 = 0.5236$.

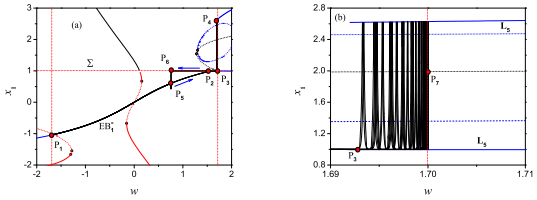

Fig. 18. Overlap of the transformed phase portrait and equilibrium branches on the (w, x_1) plane in (a) with locally enlarged part in (b) for $A = 1.70$.

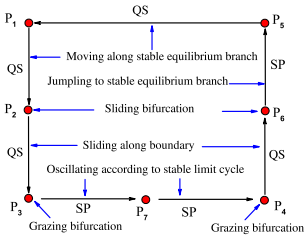

Fig. 19. Structure of the bursting attractor for $A = 1.70$.

We also turn to the overlap of the transformed phase portrait and equilibrium branches on the (w, x_1) plane to investigate the mechanism of the bursting oscillations, seeing Fig.6.

When the trajectory starts from the point P_1, at which $w = -1.70$, it moves almost strictly along the stable equilibrium branch EB_1^-, appearing in quiescent state QS_1, until it reaches the boundary at P_2, at which sliding bifurcation occurs. With the increase of w, the trajectory moves along the boundary, leading to the sliding phenomenon. When the trajectory arrives at the point P_3, it turns to oscillate according to the limit cycle L_5, leading to spiking state SP_1 via grazing bifurcation.

When the trajectory oscillates to P_7 with maximum w at $w = +1.70$, it turns to the left in spiking oscillations since w decreases with the increase of time. Grazing bifurcation at P_4 causes the trajectory to settle down to the non-smooth boundary to begin the quiescent state QS_2. When the trajectory moves along the boundary to the point P_6, sliding bifurcation occurs, causing the trajectory to jump to the stable equilibrium branch EB_1^- in D_-, yielding spiking oscillations SP_2. The trajectory may finally settles down to the stable equilibrium branch at P_5 and turns to move almost strictly along the branch EB_1^- until the trajectory arrives at the starting point P_1, which finishes one period of the bursting oscillations.

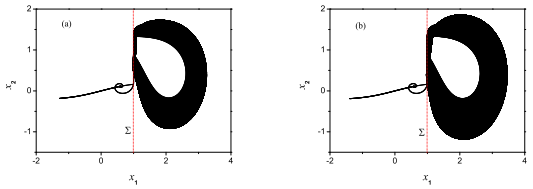

Fig. 20. Phase portrait on the (x_1, x_2) plane. (a) $A = 2.50$; (b) for $A = 3.0$.

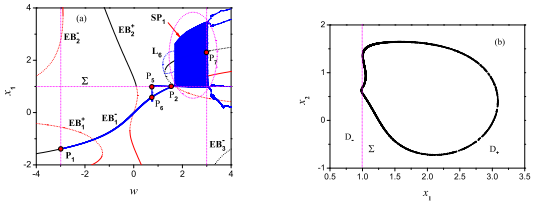

Fig. 21. (a) Overlap of the transformed phase portrait and equilibrium branches on the (w, x_1) plane for $A = 3.0$; (b) Projections of Poincaré map on the (x_1, x_2) plane with the initial condition $(x_1, x_2, x_3, x_4, t_0) = (3.3931, 0.5494, 1.8354, 0.7843, 0)$.

The structure of the bursting oscillations is shown in Fig.19, from which one may find that sliding bifurcation and grazing bifurcation cause the alternations between the quiescent states and spiking states. Therefore, the type of busting oscillations can be called non-smooth point-cycle bursting from the structure, or be called sliding/G-bifurcation bursting attractor by the bifurcations at the transitions.

4.3 Bursting attractor with one-torus spiking oscillations

More influence of the non-smooth grazing limit cycle L_5 on the bursting attractor can be found for larger exciting amplitude, seeing Fig.20 for $A = 2.50$ and $A = 3.0$.

The overlap of the transformed phase portrait and the equilibrium branches for $A = 3.0$ is presented in Fig.21a, while the related time history od x_1 and w is shown in Fig.22. From the overlap of the transformed phase portrait and equilibrium branches on the (w, x_1) plane in Fig.21a, one may find that the mechanism of the bursting oscillations is the same as that of the attractors in Fig.17. The repetitive spiking state SP_2 oscillate according to L_5 for longer interval along w-axis with larger A.

Spiking oscillations in one-torus type To reveal the characteristics of the SP_1, here we introduce the

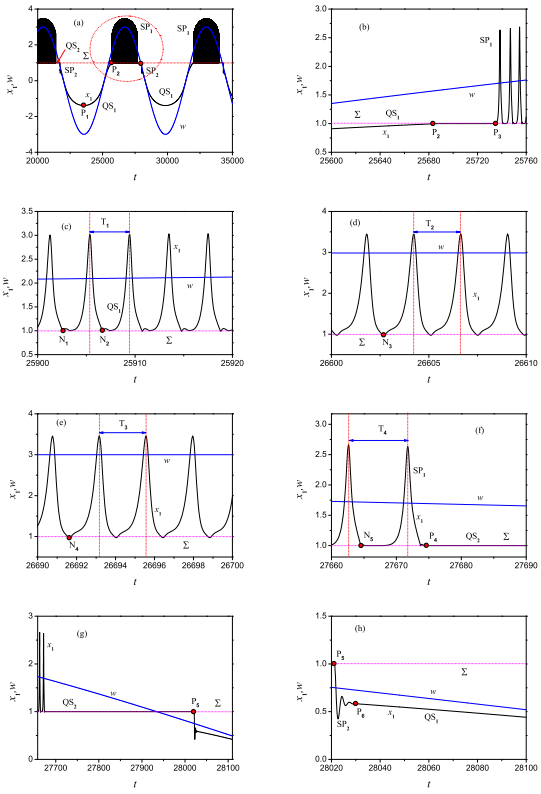

Fig. 22. Time history of x_1 for $A = 3.0$ in (a) with locally enlarged parts in (b)-(h).

Poincaré map defined by $\{[x_1(t), x_2(t), x_3(t), x_4(t)] \mid t = t_0 + 2N\pi/(\varepsilon\Omega), N = 0, 1, 2, \cdots\}$. Numerical simulations reveals that the Poincaré map behaves in a fixed point when the initial condition is taken at an arbitrary point on the trajectory not in the spiking oscillations SP_2. However, when the initial condition is taken at an point on the trajectory in the spiking oscillations SP_2, the projections of the Poincaré map on the (x_1, x_2) plane are located exactly on a cycle, which indicates that the spiking oscillation SP_2 appears in quasi-periodic form, shown in Fig.21b.

Period-decreasing and period-adding in spiking oscillations Now we focus on the time history of the x_1, presented in Fig.22. When w takes at its minimum value at P_1 with $w = -3.0$ in Fig.22a, the trajectory moves almost strictly along EB_1^- to the non-smooth boundary. Then the trajectory turn to slide along the boundary via sliding bifurcation, until grazing bifurcation occurs, which causes the trajectory to begin repetitive spiking oscillations.

For the spiking oscillations SP_1, it can be found that the slow-varying parameter w may change between $w = +1.6990$ to $w = +3.0$, which implies that spiking state may oscillate according to different non-smooth

limit cycles. Though the amplitudes may vary almost strictly according to L_5, the frequencies change with the variation of w, shown in Fig.22.

The period of the spiking oscillations may decrease when w increase from $w = 1.6990$. For example, when $w = 2.1040$, the period can be approximated at $T_1 = 4.0513$, shown in Fig.5c, while for $w = 2.9839$, the period is $T_2 = 2.3981$, seeing Fig.5d. Further investigation reveals that period-decreasing phenomenon can be observed when w increase from $w = +1.6990$ to $w = +3.0$.

On the contrary, one may find the period can be computed at $T_3 = 2.3984$ when $w = 3.0$, seeing Fig.22e, while $T_4 = 9.1890$ for $w = 1.6701$, shown in Fig.22f. which implies period-adding phenomenon can be obtained for w decreases from $w = +3.0$ to $w = +1.6990$.

When the trajectory oscillates to the boundary at P_4 in Fig.22f, it turns to move along the boundary to start the quiescent state, yielding sliding phenomenon until the effect of the sliding bifurcation occurs, which causes the trajectory to jump to the stable focus type equilibrium branch EB_1^-.

Remark: Not only the period-decreasing and period-adding phenomena, but also the grazing forms, are similar to those of the non-smooth fast subsystem, seeing Fig.8b and Fig.12, which further demonstrate that the super-cone caused by the unstable focus is one of the reasons for the period-adding and period-decreasing phenomena in non-smooth vector field. Furthermore, when the initial condition is not taken at the SP_1 stage, the projections of Poincaré map on the (x_1, x_2) plane will be located at a fixed point. Therefore, both the bursting attractors in Fig.20 are of quasi-periodic type, in which the quiescence seems to be pivot of the oscillations. implying for each period of the external excitation, the trajectory will repeat the movement in quiescent stage, while it may visit different points on the limit cycle L_5 during the spiking stage.

4.4 Bursting attractor with two-torus spiking oscillations

Note that $w \in [-A, +A]$. For $A \in (3.0656, 4.4363)$, because of the interaction between the trajectory and the non-smooth boundary, period-doubling bifurcation of the non-smooth limit cycle L_5 in FS_0 can be observed, seeing the bursting oscillations in Fig.1, which causes the qualitative change of the bursting oscillations, shown in Fig.23 for $A = 4.0$. The spiking oscillations SP_1 in Fig.23b can be further divided into two segments approximated by $w = w_{pd} \approx 3.2622$, in which the part R corresponds to the oscillations according to the period-2 limit cycle bifurcated from L_5, while the

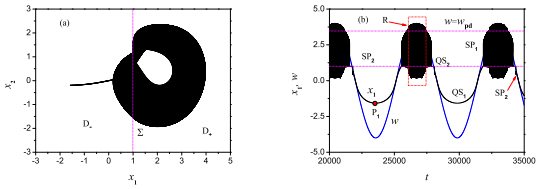

Fig. 23. Bursting oscillations for $A = 4.0$. (a) Phase portrait on the (x_1, x_2) plane; (b)Time history of x_1 and $w = A\sin(0.001t)$.

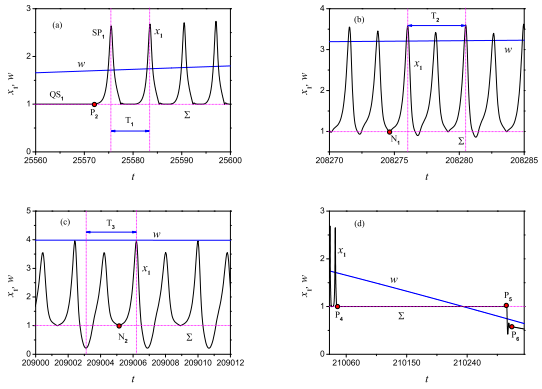

Fig. 24. Locally enlarged parts of time history of x_1 and $w = A\sin(0.001t)$.

other oscillate according to the limit cycle L_5, seeing Fig.23b.

From the locally enlarged parts of time history of x_1 plotted in Fig.24, one may find the frequency of repetitive spiking oscillations in SP_1 changes with the variation of w. When the trajectory begin to spike at P_2 in Fig.24a, the frequency of the oscillations can be computed at $\omega_1 = 2\pi/T_1 = 0.7893$. It increases with the increase of w because of period-decreasing phenomenon until period-doubling bifurcation occurs at $w = w_{pd}$ with the frequency approximated at 2.7312. The frequency changes to be $\omega_2 = 2\pi/T_2 = 1.3962$ at $w = 3.217$, shown in Fig.24b, which increases to $\omega_3 = 2\pi/T_3 = 2.02683$ at $w = 4.0$, shown in Fig.24c.

Therefore, the period-decreasing or increasing phenomenon not only exists in the oscillations according to L_5, but also exists in the oscillations according to the period-2 cycle bifurcated from L_5.

The mechanism of the bursting attractor is similar to that for the $A = 3.0$ except that period-doubling phenomenon exists in SP_1. From the overlap of the transformed phase portrait and the equilibrium states of the fast subsystem in Fig.25, one may find, when the trajectory starting from P_1 in Fig.25a with $w = -4.0$, it moves almost strictly along EB_1^- to the boundary at P_2 in Fig.25b. Sliding bifurcation causes the trajectory

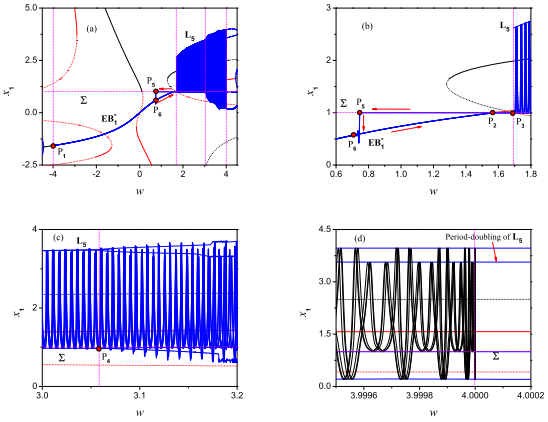

Fig. 25. Overlap of the transformed phase portrait and the equilibrium states in (a) with locally enlarged parts in (b)-(d).

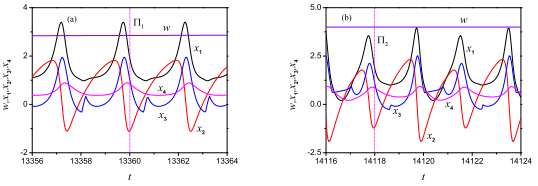

Fig. 26. Cross-sections for the Poincaré maps.(a) Π_1 at $(x_1, x_2, x_3, x_4, t_0) = (1.9275, -1.0682, 0.9604, 0.8542, 13360.)$; (b) Π_2 at $(x_1, x_2, x_3, x_4, t_0) = (2.0113, -1.1731, 1.1562, 0.8909, 14118.)$. The cross-section Π_1 is located at the region associated with the stable period-1 limit cycle L_5, while the cross-section Π_2 corresponding to period-2 cycle bifurcated from L_5 via period-doubling bifurcation.

to move along the boundary until grazing bifurcation occurs P_3 in Fig.25b, at which spiking oscillations SP_1 according to L_5 take place.

The trajectory oscillating according to L_5 turns to oscillate according to the period-2 cycle when period-doubling bifurcation occurs at P_4 in Fig.25c. When the trajectory returns when w reaches its maximum value with $w = +4.0$, seeing Fig.25d. Period-doubling bifurcation causes the trajectory to move oscillate according to L_5 until grazing bifurcation takes place at P_3, which causes the trajectory to sliding along the boundary. When the trajectory moves to P_5, the effect of sliding bifurcation appears, leading to the jumping phenomenon. The trajectory finally settles down to EB_1^- at P_6 in Fig.25b. When the trajectory moves along EB_1^- to the starting point P_1, one period of the excitation is finished.

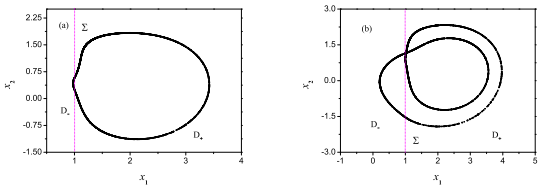

Fig. 27. Poincaré maps on the (x_1, x_2) plane with different cross-sections for $A = 4.0$. (a) Projections on the cross-section Π_1; (a) Projections on the cross-section Π_2.

To reveal the property of the oscillations, we also introduce the Poincaré map defined by $\{[x_1(t), x_2(t), x_3(t), x_4(t)] \mid t = t_0 + 2N\pi/(\varepsilon\Omega), N = 0, 1, 2, \cdots\}$. When the initial point is taken at the point on the trajectory in quiescent state, the Poincaré map appears in a fixed point, which demonstrate that the trajectory will repeat the movement of quiescence for each period of the external excitation. Here we take two cross-sections for the trajectory in spiking state SP_1, corresponding to period-1 and period-2 limit cycles, respectively, shown in Fig.26.

The projections of the Poincaré maps on the cross-section Π_1 and Π_2 are presented in Fig.26, which show that the quasi-periodic spiking oscillations change between two tori in turn, divided by the period-doubling bifurcation point at $w = w_{pd}$.

Remark: By skipping long enough the transient process, for each period of the excitation, numerical simulations shows that the trajectory visits the same point it is in quiescent state. However, The trajectory may visit different points located on the related period-1 and period-2 limit cycles, implying the spiking stage is composed of two segments, during which the trajectory oscillates according to two limit cycles. Furthermore, the trajectory in SP_2 is repeated in each period, which can be approximated by the transient process from the point P_5 on the boundary to the stable focus P_6 on EB_1^-.

4.5 Bursting oscillations with three-torus spiking oscillations

When the exciting amplitude increases to $A = 4.4363$, which implies super-critical Hopf bifurcation may occur at $w = -4.4663$, leading to qualitative change of the structure of bursting oscillations, seeing Fig.28 for $A = 5.0$. The trajectory oscillates around two cycles, seeing Fig.28a, which can be divided into six segments corresponding to three stages of quiescent states and

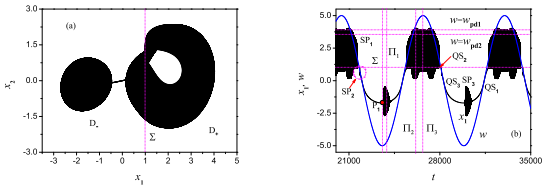

Fig. 28. Bursting oscillations for $A = 5.0$. (a) Phase portrait on the (x_1, x_2) plane; (b)Time history of x_1 and $w = A\sin(0.001t)$.

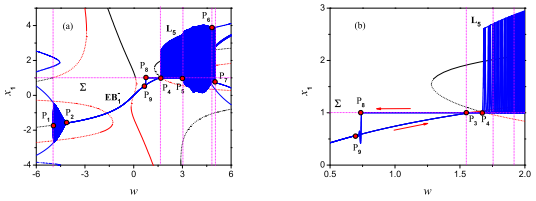

Fig. 29. Overlap of the transformed phase portrait and the equilibrium states of the fast subsystem in (a) with locally enlarged part in (b).

spiking states, respectively, denoted by QS_i and SP_i with $i = 1, 2, 3$, shown in Fig.28b.

The mechanism can be obtained by the overlap of the transformed phase portrait and the equilibrium states of the fast subsystem, plotted in Fig.29. The trajectory, starting from P_1 with $w = -5.0$, behaves in spiking oscillations SP_3, which settles down to EB_1^- at P_2 via super-critical Hopf bifurcation to begin the the quiescence QS_1, shown in Fig.29a.

The trajectory moves almost strictly along EB_1^- to the boundary Σ at P_3, at which sliding bifurcation occurs, causing the trajectory to sliding along Σ to P_4. It turns to spike according to the non-smooth limit cycle L_5 via grazing bifurcation, represented by SP_1. The trajectory may oscillate according to a period-2 cycle during the interval between P_5 and P_6, corresponding to the period-doubling and reverse period-doubling bifurcation points, respectively, shown in Fig.29a.

The trajectory then oscillates according to L_5 until w reaches its maximum value at P_7 with $w = +5.0$. Similar behaviors can be observed for the trajectory to return from P_7 to P_4. The trajectory changes to slide along Σ via grazing bifurcation. When the trajectory in QS_2 state moves to P_8 along Σ, it jumps to EB_1^- for the effect of sliding bifurcation.

Repetitive spiking oscillations SP_2 can be observed, which may quickly settle down to the focus-type EB_1^- to begin the quiescence QS_3. It turns to oscillate according to L_1 via Hopf bifurcation at P_1 to begin the

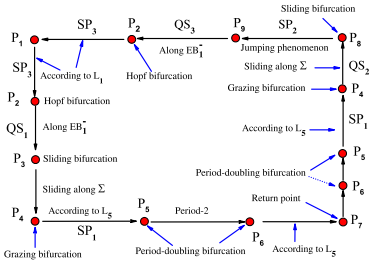

Fig. 30. Bursting structure for $A = 5.0$.

spiking oscillations SP_3. When the trajectory arrives at P_1, one period of excitation is finished, seeing Fig.29b.

The structure of the bursting attractor can be described by Fig.30, from which one may find that the trajectory may oscillate around a stable focus and two limit cycles. Though one of the cycles may change between period-1 and period-2 types, and sliding phenomenon along the boundary can also be observed, the form of bursting oscillations can be called quasi-periodic 1-point/2-cycle bursting attractor from the structure. Of course, we can also name the bursting oscillations by the bifurcations at the alternations between the quiescent states and spiking states.

Further investigation reveals that the trajectory repeat its route when it is in quiescent states. However, it does not repeat its route when the trajectory behaves in SP_1 and SP_2, seeing the locally enlarged part of the transformed phase portrait plotted in Fig.29b, similar to that in Fig.25d.

To reveal the property of the spiking oscillations, we chose three cross-sections, denoted by $Pi_i (i = 1, 2, 3)$, shown in Fig.28b. The projections of the Poincaré map at the three cross-sections, defined by $\{[x_1(t), x_2(t), x_3(t), x_4(t)] \mid t = t_0 + 2N\pi/(\varepsilon\Omega), N = 0, 1, 2, \cdots\}$ on the (x_1, x_2) plane are presented in Fig.31.

It can be found that the projections of the map at the three cross-sections are located on different cycles, respectively, which demonstrates that both SP_1 and SP_3 are quasi-periodic. Furthermore, SP_1 can be divided into two segments, corresponding to the quasi-periodic oscillations associated with period-1 and period-2 cycles, respectively.

Remark: The phenomenon does not violate the theorem of the existence and uniqueness of a solution of a differential equation, since the trajectory visit the same point in the phase space with different time.

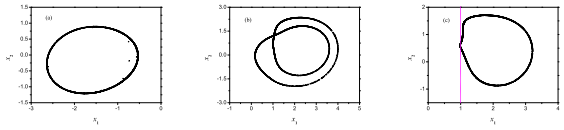

Fig. 31. Projections of the Poincaré maps on the (x_1, x_2) plane with different cross-sections for $A = 5.0$. (a) Projections on the cross-section Π_1 with initial condition $(x_1, x_2, x_3, x_4, t_0) = (-2.5031, 0.2742, 2.2182, -0.6521, 23800)$; (b) Projections on the cross-section Π_2 with initial condition $(x_1, x_2, x_3, x_4, t_0) = (3.7991, -0.6252, 2.5572, 0.8391, 26104)$; (c) Projections on the cross-section Π_3 with the initial condition $(x_1, x_2, x_3, x_4, t_0) = (2.5143, 1.5292, 0.9315, 0.5825, 25637)$.

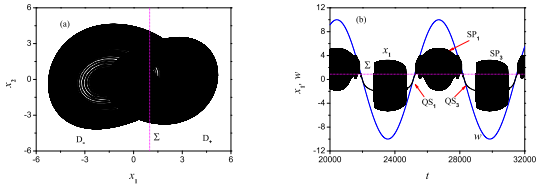

Fig. 32. Bursting oscillations for $A = 10.0$. (a) Phase portrait on the (x_1, x_2) plane; (b)Time history of x_1 and $w = A\sin(0.001t)$.

4.6 Bursting oscillations with four-torus spiking oscillations

Further increase of the exciting may cause the influence of C-bifurcation at $w = -6.8203$ involve the bursting oscillations, which may change the bursting structure, seeing Fig.32 for $A = 10.0$. The parts related to the original two limit cycles L_1 and L_5 for $A = 5.0$ develop to occupy more phase space when $w = 10.0$. The trajectory for $A = 10.0$ can also be divided into six segments, where the parts $QS_{1,2,3}$ and $SP_{1,2}$ behave in qualitative the same as those for $A = 5.0$, while great change can be observed between the segment SP_3 comparing the two cases for $A = 5.0$ and $A = 10.0$, which can be observed obviously for the related time histories of x_1 in Fig.28b and Fig.32b.

Now we focus on the SP_3 in Fig.32b. From the locally enlarged part of the time history presented in Fig.32d, one may find SP_3 can be further divided into two segments by the C-bifurcation, which oscillate according to L_1 and L_3, respectively, seeing the projections of the Poincaré may on the (x_1, x_2) plane for the two segments in Fig.34.

Further simulation reveals that the frequency in SP_3 changes very slowing with the evolution of time, which

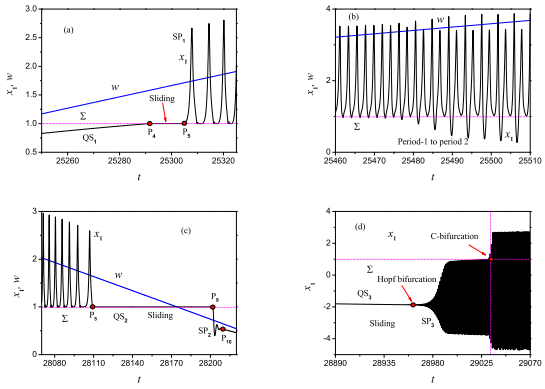

Fig. 33. Locally enlarged parts of the time history of x_1 in Fig.32b.

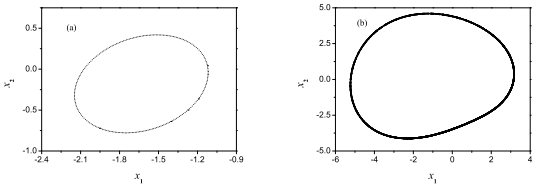

Fig. 34. Projections of the Poincaré maps on the (x_1, x_2) plane with different initial conditions for $A = 10.0$. (a) Projections with the initial condition $(x_1, x_2, x_3, x_4, t_0) = (-1.5305, -0.9038, 1.2701, -0.3751, 24680.0)$; (b)Projections with the initial condition $(x_1, x_2, x_3, x_4, t_0) = (3.1578, 0.8287, 2.6466, -0.1654, 23441)$.

agrees well with the result related to the properties of L_1 and L_3

Remark: The C-bifurcation results in the abrupt change of the amplitude of the spiking oscillations, which can be checked by the theory of non-smooth dynamics, referring to dynamical behaviors of the non-smooth generalized autonomous fast subsystem FS_0.

Now we employ the overlap of the transformed phase portrait and the equilibrium states of the fast subsystem, plotted in Fig.34, to investigate the mechanism of the oscillations.

The trajectory, starting from P_1 with $w = -10.0$, oscillates according to L_3 in spiking state SP_3 to the point P_2, at which C-bifurcation occurs, causing the trajectory to oscillate according to L_1, shown in Fig.34. Dramatic decrease of the oscillating amplitude can be observed. Further increase of w leads to the gradual decrease of the amplitude of the spiking oscillations, until Hopf bifurcation takes place at P_3. causing the trajectory to move almost strictly along EB_1^-.

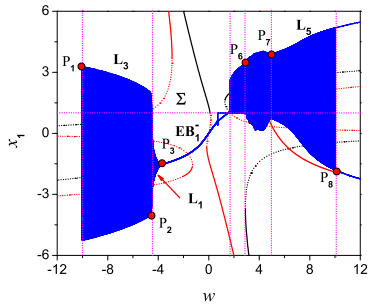

Fig. 35. Overlap of the transformed phase portrait and the equilibrium states of the fast subsystem.

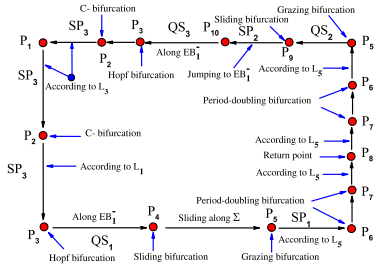

Fig. 36. Bursting structure for $A = 10.0$.

Since the movement of the trajectory from P_3 is similar to that for $A = 5.0$ until it return to P_3, which we omit here for simplicity. Therefore, the structure of the attractor can be described in Fig.35.

Numerical simulations reveals that the projections of the Poincaré of the attractor on the (x_1, x_2) plane may change between five forms, i.e., a fixed point, two limit cycles in L_1 and L_3 forms, and a period-1 or period-2 limit cycle associated with L_5, depending on the initial conditions. Therefore, it is a quasi-periodic bursting attractor associated with four tori.

Hopf bifurcation and sliding bifurcation, together with the grazing bifurcation yield the alternations between quiescent states and spiking states on the trajectory. Therefore, the type of movement can be called quasi-periodic Hopf/sliding/grazing bursting oscillations by the bifurcations. Note that the trajectory may oscillate around the four limit cycles L_1, L_3, L_5 and the cycle bifurcated from L_5 via period-doubling bifurcation, together with the equilibrium branch EB_1^1 and the non-smooth boundary Σ, it can also be called quasi-periodic non-smooth 1-point/4-cycle bursting attractor.

Further increase of the exciting amplitude can not change the topological structure of the bursting oscillations since no further bifurcation may involve the vector field, which can also be demonstrated by the numerical simulations.

5 Conclusions and discussions

For a relative high dimensional non-smooth system, there exist different coexisted attractors, which may undergo different conventional and non-conventional bifurcations. When an external excitation is introduced with the exciting frequency far less than the natural frequency, several novel bursting attractors may appear because of the influence of the coexisted attractors and the bifurcations. For the model in the paper, when the trajectory does not pass across the boundary, the system behaves in periodic oscillation with no slow-fast effect since it is governed by a smooth subsystem. With the increase of exciting amplitude, sliding bursting attractor can be observed because of the sliding bifurcation of the boundary equilibrium point, which may evolve to periodic point-cycle bursting and quasi-periodic point-cycle bursting with the further increase of the exciting amplitude. The quasi-periodic bursting may behave in mixed-torus type, in which the number of torus may change from one to four, depending on the number of stable limit cycle involved. Because of the super-cone structure defined by the flow around the unstable focus, period-adding/dcresing phenomenon can be observed when the trajectory oscillates according to set of super-cones surrounding an unstable focus-type equilibrium branch. Here we would like to suggest that for a periodically excited system with the coupling of multiple scales, we need to use different initial conditions to compute the Poincaré map for the property of the bursting oscillations, since there may exists different forms of Poincaré map.

Acknowledgement

The work is supported by the National Natural Science Foundation of China (Grant Nos. 11972173, 11632008).

Data availability statement

The data sets generated during and/or analysed during the current study are available from the corresponding author on reasonable request.

Conflict of interest

No conflict of interest exits in the submission of this manuscript, and manuscript is approved by all authors

for publication. I would like to declare on behalf of my co-authors that the work described was original research that has not been published previously, and not under consideration for publication elsewhere, in whole or in part. All the authors listed have approved the manuscript that is enclosed.

References

1. Watts, M., Tabak, J., Zimliki, C., Sherman, A. Bertram, R.: Slow variable dominance and phase resetting in phantom bursting. J. Theoret. Bio. **276**, 218-228 (2011)
2. Izhikevich, E. M.: Weakly pulse-coupled oscillators, FM interactions, synchronization, and oscillatory associative memory. IEEE Trans. Neural Networks **10**, 508C526 (1999)
3. Van der Pol, B.: On relaxation oscillations. Phil. Mag. **2**, 978-992 (1926)
4. Hodgkin, A. L., Huxley, A. F.: A quantitative description of membrane current and application to conduction and excitation in nerve. J. Physi. **117**, 500-544 (1952)
5. Ermentrout, G. B., Kopell, N.: Subcellular oscillations and bursting. Math. Biosci. **78**, 265–291 (1986)
6. Krischer, K., Luebke, M., Eiswirth, M., Wolf, W., Hudson, J. L., Ertl, G.: A hierarchy of transitions to mixed mode oscillations in an electrochemical system. Phys. D **62**, 123-133 (1993)
7. Desroches, M., Guckenheimer, J., Krauskopf, B., Kuehn, C., Osinga, H. M., Wechselberger, M.: Mixed-mode oscillations with multiple scales. SIAM Review **54**, 211-288 (2012)
8. Fenichel, N.: Asymptotic stability with rate conditions. Indiana Univ. Math. J. **23**, 1109-1137 (1974)
9. Fenichel, N.: Asymptotic stability with rate conditions II. Indiana Univ. Math. J. **26**, 81–93 (1977)
10. Lagerstrom, P. A.: Matched Asymptotic Expansions: Ideas and Techniques. Springer-Verlag, New York (1988)
11. Mishchenko, E. F., Rozov, N. K.: Differential Equations with Small Parameters and Relaxation Oscillations. Plenum Press, New York (1980)
12. Hirsch, M. W., Pugh, C. C., Shub, M.: Invariant Manifolds. Springer-Verlag, New York (1977)
13. Rinzel, J.: Bursting oscillation in an excitable membrane model in Ordinary and Partial Differential Equations. Springer Berlin Heidelberg (1985)
14. Medetov, B., Weiβ, R. G., Zhanabaev, ZZh., Zaks, M. A.: Numerically induced bursting in a set of coupled neuronal oscillators. Commun. Nonlinear Sci. **20**, 1090-1098 (2015)
15. Rinzel, J., Lee, Y. S.: Dissection of a model for neuronal parabolic bursting. J. Math. Biol. **25**, 653-675 (1987)
16. Bertram, R., Rubin, J. E.: Multi-timescale systems and fast-slow analysis. Math. Biosci. **287**, 105-121 (2017)
17. Izhikevich, E. M.: Neural excitability, spiking and bursting. Int. J. Bifurc.Chaos **6**, 1171-1266 (2000)
18. Fujimoto, K., Kaneko, K.: How fast elements can affect slow dynamics. Physica D **180**, 1-16 (2003)
19. Shimizu, K., Saito, Y., Sekikawa, M., Inaba, N.: Complex mixed-mode oscillations in a Bonhoeffer-van der Pol oscillator under weak periodic perturbation. Physica D **241**, 1518–1526 (2012)
20. Bi, Q. S., Zhang, R., Zhang, Z. D.: Bifurcation mechanism of bursting oscillations in parametrically excited dynamical system. Appl. Math. Comput. **243**, 482-491 (2014)
21. Bi, Q. S., Li, S. L., Kurths, J., Zhang, Z. D.: The mechanism of bursting oscillations with different codimensional bifurcations and nonlinear structures. Nonlin. Dyn. **85**, 993-1005 (2016)
22. Han, X. J., Bi, Q. S., Ji, P., Kurths, J.: Fast-slow analysis for parametrically and externally excited systems with two slow rationally related excitation frequencies. Phys. Rev. E **92**, 1-12 (2015)
23. Zhang, X. F., Wu, L., Bi, Q. S.: Bursting phenomena as well as the bifurcation mechanism in a coupled BVP oscillator with periodic excitation. Chinese Phys. B **25**, 70501-70507 (2016)
24. Han, X. J., Bi, Q. S.: Bursting oscillations in Duffing's equation with slowly changing external forcing. Commun. Nonlinear Sci. **16**, 4146-4152 (2011)
25. Zhang, Z. D., Li, Y. Y., Bi, Q. S.: Routes to bursting in a periodically driven oscillator. Phys. Lett. A **377**, 975-980 (2013)
26. Bi, Q. S., Ma, R., Zhang, Z. D.: Bifurcation mechanism of the bursting oscillations in periodically excited dynamical system with two time scales. Nonlin. Dyn. **79**, 101-110 (2015)
27. Han, X. J., Xia, F. B., Ji, P., Bi, Q. S.: Hopf-bifurcation-delay-induced bursting patterns in a modified circuit system. Commun. Nonlinear Sci. **36**, 517-527 (2016)
28. Simpsona, D. J. W., Meiss, J. D.: Aspects of bifurcation theory for piecewise-smooth, continuous systems. Physica D **241**, 1861-1868 (2012)
29. Oleg Makarenkov, O., Lamb, J. S. W.: Dynamics and bifurcations of nonsmooth systems: A survey. Physica D **241**, 1826-1844 (2012)
30. Leine, R. I., Van Campen, D. H., Van de Vrande: Bifurcations in nonlinear discontinuous systems. Int. J. Nonlinear Dyn. Chaos Eng. Syst. **23**, 105-164 (2000)
31. Leine, R. I.: Bifurcations of equilibria in non-smooth continuous systems. Physica D **223**, 121-137 (2006)
32. Colomboa, A., Bernardo, M., Hoganb, S. J., Jeffrey, M. R.: Bifurcations of piecewise smooth flows: Perspectives, methodologies and open problems. Physica D **241**, 1845-1860 (2012)
33. Castroa, J., Alvarez, J, Verduzcoc, F., Palomares-Ruiz, E.: Chaotic behavior of driven, second-order, piecewise linear systems. Chaos, Solitons & Fractals **105**, 8-13 (2017)
34. Medrado, J. C., Torregrosa, J.: Uniqueness of limit cycles for sewing planar piecewise linear systems. J. Math. Anal. Appl. **431**, 529-544 (2015)
35. Vaidyanathan, S., Sambas, A., Mujiarto, Mamat, M., Wilarso, Sanjaya, M. W. S., Sutoni, A., Gunawan, I.: A new 4-D multistable hyperchaotic two-scroll system, its bifurcation analysis, synchronization and circuit simulation. J. Phys.: Conf. Ser. **1764**, 012206 (2021)